Indian Journal of Engineering & Materials Sciences
Vol. 27, April 2020, pp. 256-266

Microspheres based on black sand mineral as a photocatalyst for photocatalytic hydrogen production under UV light

Andrés López-Vásquez[a*], Alis Pataquiva-Mateus[b] & Pilar Delgado-Niño[c]

[a] Department of Chemical Engineering, Universidad Nacional de Colombia, Manizales 170003, Colombia

[b]Department of Engineering, Faculty of Natural Science and Engineering, Universidad de Bogotá Jorge Tadeo Lozano, Bogotá 110311, Colombia

[c] Department of Environmental Engineering, Faculty of Engineering, Universidad Libre Sede Principal, Bogotá 111071, Colombia

Received: 03 October 2019; Accepted:22 January 2020

Frequently, black sand from coastal deposits is a magnetic ore with a complex structure that is composed principally by iron, titanium and silica oxides, and metals such as vanadium, chromium, nickel, strontium, etc. This material could be used in oxidation/reduction processes as a photocatalyst doped naturally. However, its surface area low and the mass transfer constraints caused by the cluster formation in bulk reaction due to its magnetic character, limits the photocatalytic performance. Microspheres of black sand have been prepared by a simple associating method with alginate-Na and calcined under oxidizing atmosphere at 1100 °C. These have been characterized by XRF spectroscopy, scanning electron microscopy/energy dispersive X-ray spectroscopy, Brunauer-Emmett-Teller surface area analysis, XRD diffraction, N_2 adsorption/desorption measurements, FT-IR spectroscopy, differential thermal thermogravimetric analysis, and UV-Vis spectrophotometry. The catalytic activity for photocatalytic hydrogen production from EDTA solutions under UV light irradiation, using the response surface methodology in order to determine the optimum conditions of the process, has been tested. At calcination temperature, rounded microspheres with rough surface, have had apparent density different from the raw material and although the specific surface of the microspheres decreased owing to surface sintering, the chemical composition has been similar compared with the starting material. Due to their buoyancy in the suspension, the hydrogen production due to the contact between photons that entered into suspension and the as-prepared microspheres, has been favored.

Keywords: Hydrogen production, Ilmenite-black sand, Microspheres, Mineral-based photocatalyst, Response surface methodology

1 Introduction

The photocatalytic hydrogen production based on semiconductors has been an important research field since the developments presented by Fujishima *et al.* on photoelectro chemical splitting of water[1]. This technology is one of the most promising techniques to obtain hydrogen[2] and therefore, the studies have focused on the development of new photochemical mechanisms that lead to improve its yield[3]. However, there are some limitations with respect to electron/hole pair recombination, the development of reverse reaction, and the use of a specific wavelength (generally UV range) to activate the semiconductor[4,5]. In order to overcome these restrictions at the structural level, they have been expanding strategies which consisted in the addition of electron donors, doping with noble metals, coupling semiconductors, dye sensibilization, and inhibition of the reverse reaction, among others[6,7]. Regarding surface modifications to improve the mass transfer in a bulk reaction, it has been demonstrated that maximizing the area of the structure increases the number of photons which are absorbed by the semiconductor and therefore, it results in high photocatalytic efficiency[8]. Other important aspect to the performance of the semiconductor is the crystallinity, *e.g.*, the optical band gap (E_g) value for amorphous and crystalline phases (anatase and rutile) of titanium dioxide (TiO_2) are 3.5, 3.2 and 3.0 eV, respectively[9,10]. Although the anatase absorbs light of a short wavelength range, it provides high photocatalytic activity due to the high density of localized states, resulting in surface-adsorbed hydroxyl radicals and slower electron/hole recombination rate relative to rutile[11–13]. Clearly, it means that the performance of the photocatalyst depends on its morphology, crystal structure, and crystallite size.

Whereas the use of ores in heterogeneous catalysis in mineral surfaces is shown as an option to develop oxidation/reduction processes such as photovoltaic cells, water purification systems, or hydrogen production[14–17], the application of these potential

*Corresponding autor (E-mail: aflopezv@unal.edu.co)

semiconductors is modest and little references are available in the literature. Within these, black sand is a mineral that is composed by a rich mixture of photocatalytic interest oxides (Fe_2O_3, TiO_2, SiO_2, etc.) whose composition varies geographically[18–21]in form of sediments of igneous rocks in deposits that are present in the riverbeds and coastal areas. The morphologies of their irregular blocks are denoted by numerous etch mark probably formed by mechanical abrasion and might have been brought to the riverbeds due to reworking of bottom sediments. This geological condition generates a material with low surface area and porosity, whose photocatalytic mechanism is not favored due to mass transfer limitations affecting the adsorption phenomenon (interaction radical-substrate). A strategy to increase the surface area could be the size reduction by mechanic milling process, forming particles with a diameter smaller than the wavelength of the incident light, but they are not optically transparent due to particles that scatter the light[22]. Moreover, difficulties in maintaining the mineral slurry due to high density, reduce the optical path as a result of the turbidity and darkness of the suspension, reducing the electron/hole pair generation rate[23].

As mentioned above, the crystallinity and structure of the catalytic system could affect the activity and selectivity and in this sense, a wide variety of nanostructured materials with different morphologies, including the microspheres[24–26], have been developed to produce highly active photocatalysts. These modifications improve the hydrodynamics of the particles and the light scattering could be reduced, increasing the optical depth of photons that pass through the bulk reaction. One might expect that the catalyst disposed in microspheres with characteristics such as low density and porosity, must have a high activity during the development of the photocatalytic process[27]. In this sense, several solid and liquid species used as photocatalysts, have been immobilized by microencapsulation techniquesusing a water-soluble polymer (sodium alginate). By this versatile method of aqueous-based gel formation in the presence of divalent cations (calcium chloride), a solid matrix of varied size can be obtained, which turns out to be stable at low pH values[28–32]. An important step in the formation process is the calcination temperature to which the microspheres could be prepared, since it is a determining factor in the crystalline modification of the active phases of the compounds that are present in the raw material.

On the other hand, hydrogen production depends among other, on the factors such as pH, substrate concentration (EDTA) and catalysts dose (microspheres)[33–35]. In most cases, the activity of the photocatalyst has been studied throughout “one factor at a time” methodology, while the rest of studied parameters remain constant[36]. The main limitation of this method, is that the results obtained to describe the general performance of the process, might be different from the entire study because the combined effect between variables is not consider and consequently, the optimal conditions are more difficult to predict[37–40].

To overcome this limitation, the optimization using response surface methodology (RSM) consider these interaction by the combination of several factor levels, optimizing the process[41–45]. An option is using a block-grouped Box-Behnken design (BBD) to adjust more simply, a second or third grade model to describe the photocatalytic mechanism. Generally, with this type of design the performance of the model within the studied range is improved, because the variability of responses by factors that could not be controlled, such as the interaction of photons with the surface of the photocatalyst, could be reduced. Assuming that the effects of the block based on the alias structure are additive, just a single change in the dependent variable is generated, and there is no interaction between the blocking variable and the rest of the factors[46] improving the variance and covariance of the estimated parameters[47]. The use of BBD provides anenough profile to test the goodness of the fit and it spherical design structure, not allows to evaluate extreme positions, limiting the design to range studied with physical meaning for the photocatalytic system.

In this work, the as-prepared microspheres based on black sand mineral with sodium alginate were calcined at 1100°C. The textural (crystallinity, composition of crystal phase, crystallite size, porosity, etc.) and optical properties as well as the photocatalytic activity for hydrogen production under UV light irradiation have been investigated systematically through a Box-Benhken design.

2 Experimental

2.1 Preparation of Microspheres based on Black Sand Mineral

Black sand samples were collected directly from coastal deposits located at the beaches of Santa Marta (Magdalena, Colombia) and the preparation method for raw material was followed according to

methodology used by Lopez-Vasquez *et al.*[48]. This sample was scrubbed and scrapped, and due to its iron content, it was subject to separation applying a magnetic field of 0.0311 T to obtain a concentrated solution (M1) that was used for preparing the microspheres according to the methodology proposed by Mateus *et al.*[49]. Typically, to prepare a 2.0% solution of sodium alginate (Manucol ® DH MCLDHP, FMC Biopolymer), the polymer (without further purification), was dispersed in deionized water. After that, M1 (<53 μm) in a 7:3 w/w ratio, was added to alginate solution with constant stirring until form a homogeneous paste that was extruded dropwise into a 0.1M $CaCl_2$ crosslinking solution. The spherical particles formed were allowed to harden during 30 min. The size of the microspheres was controlled by regulating the extrusion flow rate using a single syringe infusion pump and applying a coaxial air stream of 30 Lh^{-1}(Encapsulation Unit Var 1-J1, Nisco). After gelling stage, the microspheres recovered and classified were rinsed with water to remove the remaining$CaCl_2$[49]. Finally, they were dried at 30°C, and calcined at 1100°C for 2 hrs.

2.2 Microspheres Characterization

The quantitative analysis of microspheres was performed using fluorescence spectroscopy X-ray (MagixPro PW-2440 Philips). The surface morphology was examined by using scanning electron microscopy (SEM) equipped with an EDX system for energy-dispersive spectroscopic analysis (VEGA3 TESCAN). The crystalline phases that are present were identified by patterns using an X-ray powder diffractometer (PANalytical X'Pert Pro PW 3064/60) with Cu Kα radiation. The surface area was determined through Brunauer-Emmett-Teller (BET) measured by nitrogen adsorption (100 mL min^{-1}) at 110°C K on a ChemBET PULSAR™ TPR/TPD (Quantachrome Instruments, USA). The infrared spectroscopy (Fourier transform) for bond vibration identification was measured at room temperature on a FT-IR 8400S spectrophotometer (Shimadzu) in the range of 400-4000 cm^{-1}. Thermogravimetric analysis (TGA) and thermal behavior were carried out using the TGA/DSC Star System Mettler Toledo analyzer and the optical properties were examined by means of a UV/Vis spectrophotometer equipped with integrating sphere ($BaSO_4$ as reference)for diffuse reflectance spectra acquisition (Shimadzu UV-2600).

2.3 Photocatalytic Hydrogen Production: Response Surface Methodology

For evaluating the photocatalytic activity of microspheres on hydrogen production by EDTA solutions under UV light irradiation, a series of batch experiments were carried out in a reactor (photochemical reactor ACE Glass) provided with a radiation source (70 W medium pressure Hg lamp which emits mostly UV light) located inside a cylindrical quartz vessel jacketed and coupled to a Pyrex glass vessel which was used as photoreactor (microspheres including). For aqueous solutions preparation, ethylenediaminetetraacetic acid disodium salt dihydrate (99%, MERCK,) was dissolved into ultrapure water obtained from an ELGA PURELAB Option-R apparatus (resistivity = 0.067 μS cm^{-1}). For photocatalytic tests, a known amount of microspheres (according to the experimental design) and 200 mL aqueous EDTA solution were placed into the reaction vessel. The suspension, magnetically stirred, was deaerated by bubbling N_2 gas for 30 min to remove the oxygen from the solution, and then the solution was exposed to UV light irradiation during 5 hrs. The temperature of the homogeneous suspension was kept at 25 °C by thermostatic bath with tap water attached to the quartz vessel. After the photocatalytic treatment, the products of the process were released from the reactor through the gas product outlet. A gaseous sample (basically H_2 and CO_2) was collected in a Tedlar bag and the hydrogen that was generated was measured using a gas chromatograph (Agilent 2460, Molecular sieve 5A, Nitrogen gas) equipped with a thermal conductivity detector (TCD). In order to study the effect of factors such as pH, sacrificial agent concentration, and the microspheres dose at different levels and their influence on photocatalytic hydrogen production, the response surface methodology (RSM) was applied through a Box-Benhken design.

The experimental values of photocatalytic hydrogen production under various experimental conditions are shown in Table 1, and the experimental and predicted responses are shown as well. Design Expert V.8.0.6 (Stat-Ease Inc., Minneapolis, MN, USA) software was used to explain the design by the development of a statistical analysis which include normal plot, residual analysis, the main and interaction effects, contours plot, and analysis of variance (ANOVA) determination.

Table l — Box-Behnken design with predictive/experimental values for photocatalytic hydrogen production based on as-prepared black sand microspheres.

Run	Factor			Hydrogen production (μmol)		
	pH	EDTA concentration (mM)	Microspheres dose (g L^{-1})	Experimental	Predicted	Residual
1	8.5	1.0	0.5	155.6	155.7	0.01
2	6.0	5.0	0.5	110.8	194.7	-83.9
3	3.5	1.0	0.5	140.4	140.3	0.01
4	6.0	10.0	1.0	685.6	652.5	33.1
5	6.0	5.0	0.5	242.2	194.8	47.4
6	6.0	1.0	0.1	15.11	56.4	-41.3
7	8.5	10.0	0.5	550.5	550.4	0.01
8	3.5	5.0	1.0	650.5	687.7	-37.2
9	6.0	1.0	1.0	15.5	-26.2	41.7
10	6.0	10.0	0.1	366.9	398.9	-32.0
11	8.5	5.0	0.1	490.4	453.3	37.1
12	6.0	5.0	0.5	141.2	194.7	-53.5
13	8.5	5.0	1.0	310.3	347.4	-37.1
14	6.0	5.0	0.5	239.2	194.7	44.5
15	3.5	10.0	0.5	260.7	260.6	0.01
16	6.0	5.0	0.5	240.2	194.7	45.5
17	3.5	5.0	0.1	485.4	448.2	37.2

3 Results and Discussion

3.1 As-prepared Microspheres Characterization

The results of the quantitative analysis of black sand-microspheres performed by fluorescence spectroscopy X-ray are listed in Table 2. Although the calcination process was subjected to the microspheres, the composition remained relatively constant (±2.0%) indicating no significant degradation of compounds. Considering that the Na_2O content decreased and the carbon levels were not detectable, the microspheres did not retain content of Na-alginate in their structure because it was burnt off during the calcination treatment at 1100°C.

The micrograph structures of as-prepared microspheres after sintering process are depicted in Fig. 1. Based on image processing, it was determined that the average diameter of mineral-based microspheres was 336.61 μm ±35.8 (*n=15*) (Fig. 1(a) and Fig 1(b)), and the empty space onto surface material associated to porosity was approx. 16.0% (Fig. 1(c)). By SEM observation, it was possible to identify a sintering structure as aggregates of crystallites after calcination process (Fig. 1(d)); moreover, associated mineral particles maintaining the original spherical shape. The EDX spectrum (Fig. 2) confirmed the elemental composition. The results were like those obtained from the XRF analysis in which the principal elements that are present in the mineral were Fe, Ti, Si, and Al.

Table 2 — Chemical composition of mineral samples obtained from black sand mineral (%w).

Compound and/or element	M1 (0.0331 T)	Microspheres
Fe_2O_3	86.819	84.975
TiO_2	4.548	4.427
SiO_2	2.608	6.815
Al_2O_3	1.041	1.168
MnO	0.418	0.393
ZrO_2	0.211	0.172
CaO	0.742	0.991
Na_2O	1.162	0.160
MgO	0.470	0.172
P_2O_5	0.430	0.342
V	0.188	0.171
K_2O	0.086	0.126
Cr	0.059	0.087
Trace elements (S, Zn and Sr)	1.218	N.D

ND: Non detectable

In previous work, single-point BET surface area for black sand (RM) and magnetic concentrate (M1), was determined by dynamic flow (0.5083 and 0.4928m^2g^{-1}) [48], while for microspheres (MS) was 0.3727 m^2g^{-1}. The sintered framework formed after calcination process, produced a decreasing in the specific area.

The XRD patterns of prepared materials are shown in Fig. 3.For starting magnetic concentrate, the pattern shows typical peaks for magnetite,

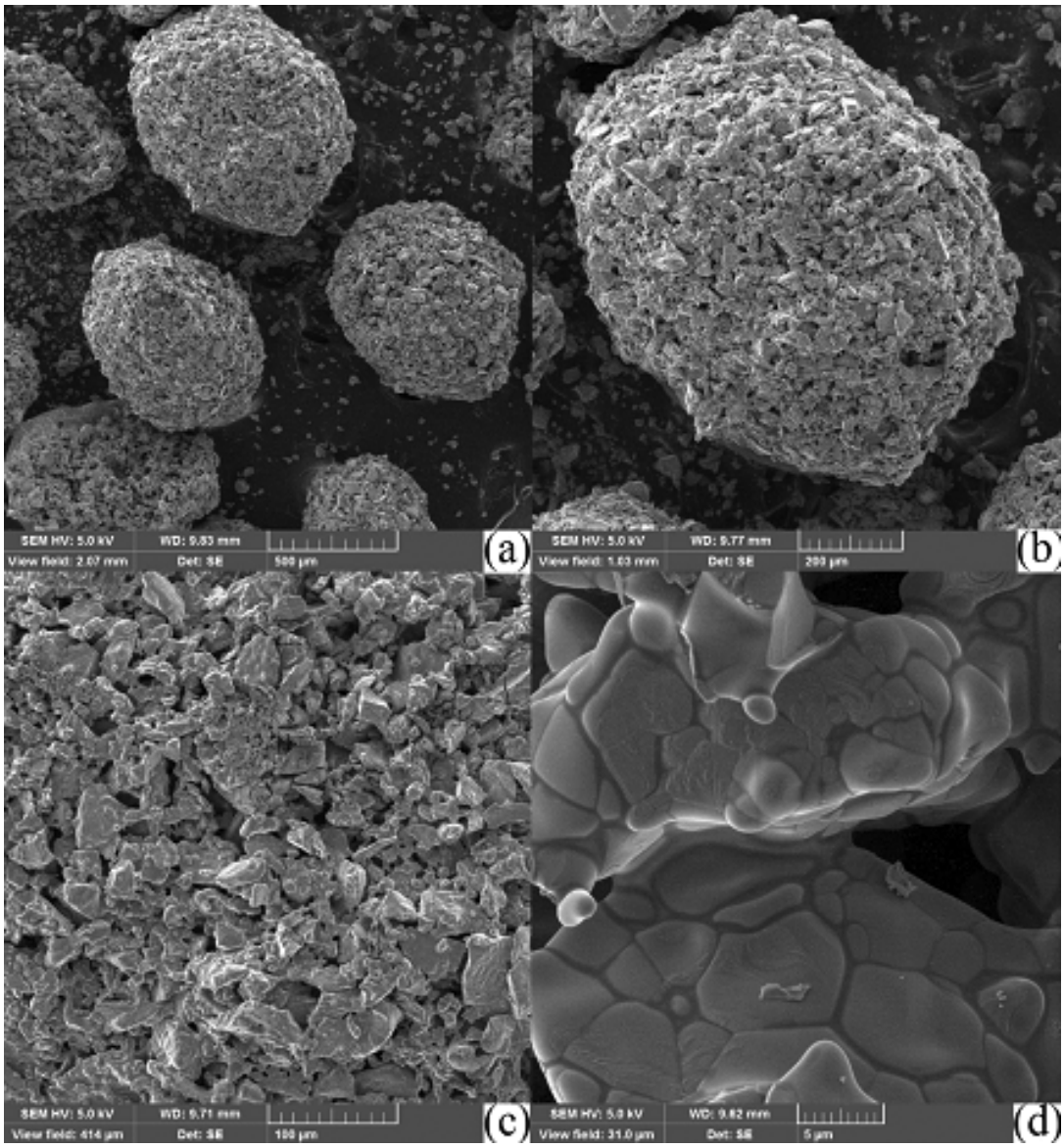

Fig. 1 — SEM micrographs of as-prepared microspheres from black sand mineral: (a) 100X, (b) 200X, (c) 500X and (d) 6700X.

ilmenite, hematite, and quartz, while the structure of the as-prepared microspheres revealed the formation of titanium oxide (Ti_3O_5) due to the phase of transitions of mineral. The diffraction peaks of impurities such as Na and C corresponding to alginate, were not observed. According to Simpraditpan *et al.*, the Na content into material, for this case the microspheres, could be diminished due to the calcination process to which they were subject[13]. The results showed that the magnetite in M1 was oxidized and the main component in MS was α-Fe_2O_3. For M1, the main magnetite diffraction peaks were detected at 18.34°, 30.12°, 35.47°, 37.11°, 43.09°, 56.98°, and 62.56°. The XRD patterns for ilmenite were observed at 43.09°, 56.98° and 62.56°, while for hematite was observed at 62.56°. For quartz, the representative peaks[50] were detected at 27.02°, 37.11°, and 43.09°. For MS, the diffraction peaks for hematite (α-Fe_2O_3) were at 24.16°, 32.56°, 35.62°, 40.87°, 49.46°, 54.08°, 57.59°, 62.43°, and 63.98°, and for the titanium oxide (Ti_3O_5) at 25.55°, 54.08°, 57.59°, 62.43°, and 63.98°.

Functional groups present into microspheres structure were confirmed by Fourier-transform infrared spectroscopy (Fig. 4). The variations in the spectra indicate the formation of alloys among its main components (Fe and Ti). In general, the main

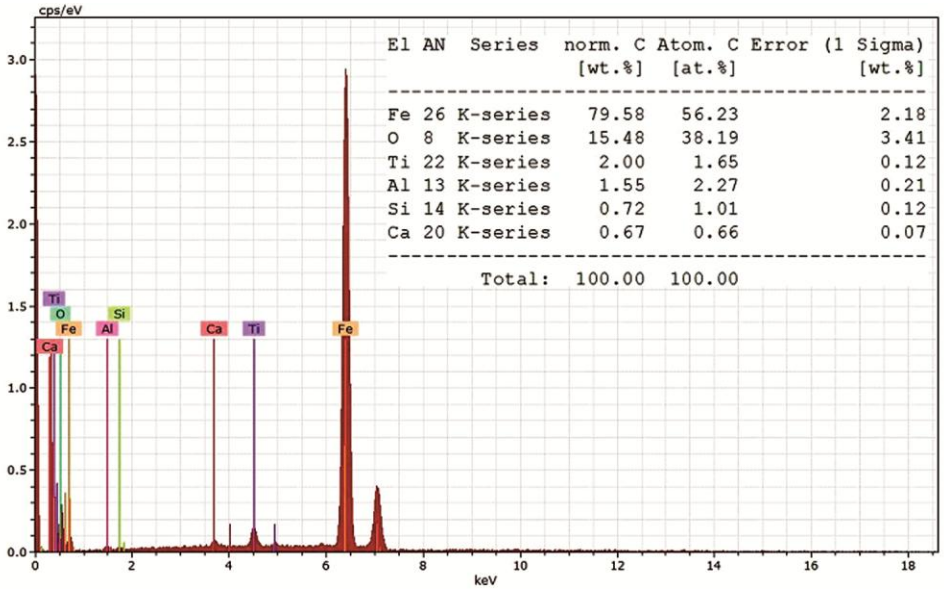

Fig. 2 — EDX spectrum of mineral-based microspheres for photocatalytic hydrogen production.

peaks could be attributed to iron oxides with slightly contributions of TiO_2 phases. The peaks presented at 2879 cm^{-1} and 1602 cm^{-1} were assigned to OH, while the vibration at 3388 cm^{-1} was related with a Si-OH mode associated with H_2O[51,52]. Frequently, the vibrational bond located at 1386 cm^{-1}, is due to symmetric and antisymmetric curvature of the O-Si-O and/or Si-O-Ti bonds presented at lower frequencies[53,54]. In the insert, one can observe the characteristic bands for the α-Fe_2O_3 (hematite) at 466 cm^{-1}, TiO_2 at 507 cm^{-1}, ilmenite at 532 cm^{-1}, and for magnetite at 573 cm^{-1} where peaks were faintlydisplaced for hematite (474 cm^{-1}) and magnetite (576 cm^{-1}), while the characteristic peak[50] for TiO_2 was at 507 cm^{-1}.

For the TGA/DSC analysis (Star System Mettler Toledo analyzer), the sample was degasified with nitrogen stream (100°C) for 1.0 h at 20 $mLmin^{-1}$. After that, the analysis was performed between 25°C – 1100°C at a heating rate of 5°C$min^{-1}$with flowing air (100 $mLmin^{-1}$). TGA/DSC curves were normalized regarding the sample weight. Fig. 5 reports the thermal stability of magnetic concentrate that was used to form the microspheres. According to the results, the microspheres possess high thermal stability reflected in low weight gain (~3.0 %) on ignition. This behavior can be attributed to the oxidation of iron compounds in oxidizing atmosphere (Fe^{2+} to Fe^{3+})[55] and phase of transformation of the compounds presents in the mineral[50]. The thermogravimetric curve can be divided into three

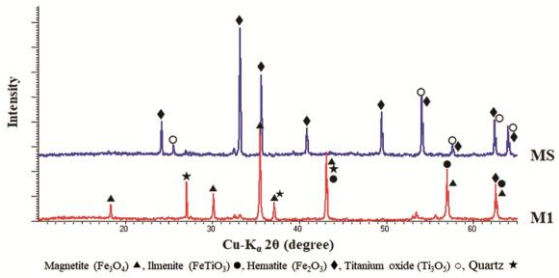

Fig. 3 — XRD patterns of the starting material (M1) and as-prepared microspheres calcined at 1100°C.

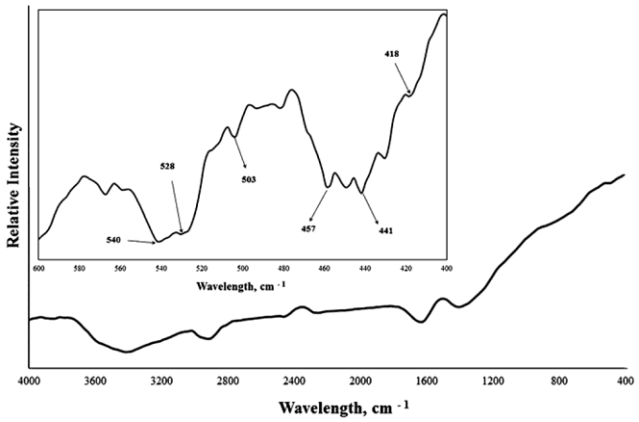

Fig. 4 — FTIR spectra for as-prepared microspheres from black sand.

stages. The slightly weight gain (<0.5%) was observed from 25°C to 200°C and could be attributed to some crystallization of magnetite (Fe_3O_4) to γ and α-hematite. The second stage (200-1000°C) was assigned to the transformation from γ to α-hematite phase (~3.0%), and from 1000°C, the material

showed a thermal stability. The DSC curve showed an exothermic peak of about 800°C and confirms the transformation process phase from crystal type γ-Fe_2O_3 (low temperature) to α-Fe_2O_3 (high temperature) [56].

UV-Vis/DR spectra for as-prepared microspheres (Fig. 6) showed a strong absorption peak at 370 nm (UV range).In order to estimate the band-gap energy (E_g), the Tauc plot was used by extrapolation of the straight line from the absorption curve to the abscissa (Fig. 7)[57]. According to the result, the as-prepared microspheres had a direct optical transition corresponding to a band gap of 2.92 eV. This means that the microspheres used as a photocatalyst can be excited under UV irradiation with a visible light response in the visible range (about 410 nm) as a consequence of some interaction between iron oxides with the other mineral compounds (TiO_2, SiO_2,Al_2O_3) that are present into thestructure.

3.2 Photocatalytic Hydrogen Production

In order to optimize the reaction conditions of the photocatalytic hydrogen production based on as-prepared microspheres from black sand, the BBD (17 experiments) was applied for the response surface modeling(Table 1). From statistical analysis, both the quadratic and the mean were suggested, as shown in Table 3.

Table 4 shows the ANOVA for response surface of quadratic model developed by the statistical analysis. According to ANOVA, *F* value implies that the model is significant (11.05). This mean that only a 0.79%could due to the noise. In the same way, like the*p*-value (0.0079) is less than 0.05, indicates that the model terms are very significant[58,59]. For the "lack of fit", *F* value (2.74) confirmed that was not significant in relation to the pure error, when *p* value is 0.1730 (>0.05), showing a model with good predictability. Due to a low coefficient of variation (C.V.=24.64), the precision and good reliability of the experimental values were acceptable moreover, Adj. R^2 value of 0.8735 also implies good predictability of the quadratic model selected. Finally, the adequate precision of 21.24 above 4.0 indicated adequate model discrimination in this analysis. The values of the *p* value for *B*, A^2, C^2, and AB^2 indicate that they are significant model terms. An empirical second-order polynomial was determined in terms of coded factors, from the experimental data(Eq. (1)).

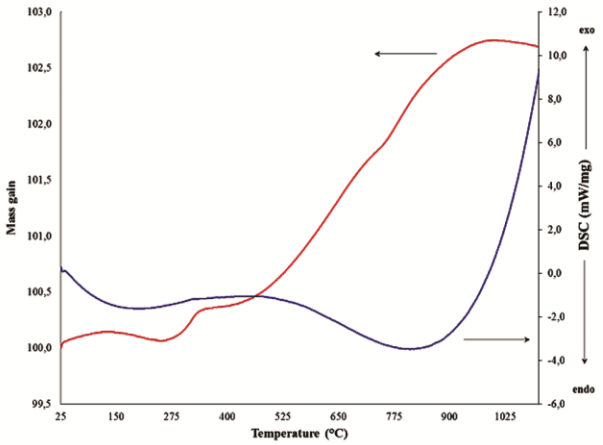

Fig. 5 — TG-DSC curves of magnetic concentrate for the preparation of microspheres from black sand.

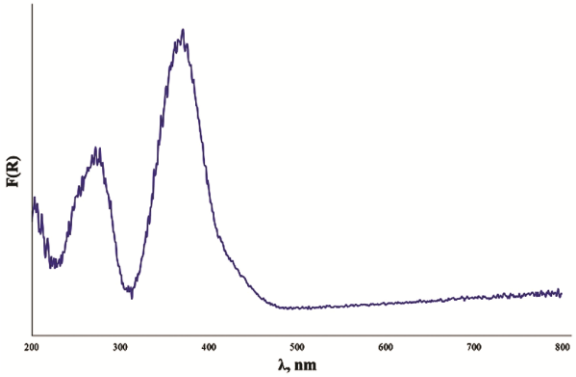

Fig. 6 — Experimental Kubelka-Munk diffuse reflectance for as-prepared microspheres based on black sand mineral.

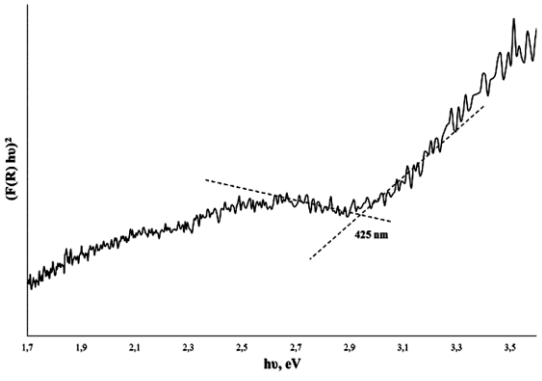

Fig. 7 — Experimental $E_g$value obtained from Tauc plot for as-prepared microspheres based on black sand mineral (direct transition).

$$y = 226.26 - 77.98A + 255.33B + 42.74C + 68.64AB - 86.32AC + 84.06BC + 141.91A\text{^}2 - 88.26\,B\text{^}2 + 132.42C\text{^}2 - 117.22A\text{^}2\,B + 144.65AB\text{^}2 \quad \ldots (1)$$

Table 3 — Sequential model sum of squares for photocatalytic hydrogen production based on as-prepared black sand microspheres.

Source	Sum of squares	Degree of freedom	Mean square	*F Value*	*p Value*	Remark
Mean	1.529×10^6	1	1.529×10^6	–	–	Suggested
Linear	3.017×10^5	3	1.006×10^5	3.36	0.0522	–
2FI	92027.72	3	30675.91	1.03	0.4200	–
Quadratic	2.026×10^5	3	67518.05	4.98	0.0371	Suggested
Cubic	78753.00	3	26251.00	6.48	0.0514	Aliased
Residual	16205.19	4	4051.30	–	–	–
Total	2.221×10^6	17	1.306×10^5	–	–	–

Table 4 — ANOVA for the response surface quadratic model for photocatalytic hydrogen production based on as-prepared black sand microspheres

Source	Sum of Squares	df	Mean square	*F* Value	*p* Value	Remark
Model	6.639×10^5	11	60351.97	11.05	0.0079	Significant
A-pH	23433.48	1	23433.48	4.29	0.0931	–
B-EDTA concentration	2.608×10^5	1	2.608×10^5	47.73	0.0010	–
C-microspheres dose	14527.01	1	14527.01	2.66	0.1639	–
AB	18844.97	1	18844.97	3.45	0.1224	–
AC	29806.12	1	29806.12	5.46	0.0667	–
BC	28435.47	1	28435.47	5.20	0.0714	–
A^2	84231.50	1	84231.50	15.42	0.0111	–
B^2	31790.77	1	31790.77	5.82	0.0607	–
C^2	71093.91	1	71093.91	13.01	0.0154	–
A^2B	27315.36	1	27315.36	5.00	0.0756	
AB^2	40324.07	1	40324.07	7.38	0.0419	
Residual	27318.75	5	5463.75	–	–	
Lack of Fit	11113.57	1	11113.57	2.74	0.1730	Not significant
Pure Error	16205.19	4	4051.30	–	–	–
Total	6.912×10^5	16	–	–	–	–
Std. dev.[a]	73.92	–	R^2	0.9605	–	–
Mean	299.95	–	Adj. R^{2b}	0.8735	–	–
C.V.[c]	24.64	–	Adeq. pre.[e].	21.24	–	–

[a] Standard deviation, [b] Adjusted R^2, [c] Coefficient of variation, [d] Predicted R^2, [e] Adequate precision. Case with leverage of 1.0000, Pred R^2 and PRESS statistic not defined

Where, y is the hydrogen production (μmol), A, B and C are the coded values terms for pH, EDTA concentration, and microspheres dose. The positive coefficients indicate that the response is favored in the high values of the respective variable between the studied ranges, whereas the negative coefficients favored it at low values. In this sense, the photocatalytic hydrogen production could be improved at a low pH, and high levels of sacrificial agent dose and microspheres. This result is consistent with the photocatalytic phenomena limited by electric attraction between the catalyst surface and substrate, and the generation of radicals mediated by the sacrificial agent. The quadratic interactions A^2 and C^2 mean that an excessive increment of these variables produces the contrary effect decreasing the hydrogen production. At low photocatalyst concentration, into bulk reaction are generated active siteswhich are available for adsorption of light and EDTA reactant, but when the photocatalyst concentration is increased attempting generate a high active sites concentration, the UV light could be scattered by all suspended material, limiting the UV light transmission. Therefore, the photocatalytic hydrogen production could decrease.

Fig. 8 shows the high correlation between the experimental and predictive values of the model in the studied range (R^2=0.9605), confirmed by the structureless pattern indicating the model sufficiency. Based on the normal probability of residuals plot (Fig. 9) and the residuals versus predicted response plot (Fig. 10), the analysis of residuals was developed.

Because most of residuals are located around the straight line, it is suggested that errors are distributed normally.

According to structure less pattern presented in Fig. 11, the quadratic model proposed by the design is satisfactory and does not violate independence neither the assumption of constant variance. Fig. 11a describes the influence of pH and EDTA concentration on the response variable while keeping the microspheres dose at 0.5 gL^{-1}. The EDTA concentration increasing under acid conditions, affects favorably the hydrogen production due to the generation of enough radicals into the suspension, responsible of water splitting. Fig. 11b describes the influence of the microspheres dose and the sacrificial agent concentration on the hydrogen production (pH at 6) and in the same way, the hydrogen production enhances with the catalyst increasing since the radicals that were formed on the microsphere surface are enough for water splitting at these concentrations. The interaction effect between microspheres dose and initial pHsolution is shown in Fig. 11c. An increase of the pH above the zero point of the proton condition of mineral (pH_{ZPC}=2.7), leads the microsphere surface to be negatively charged, resulting in an electrostatic repulsion with the EDTA dissociated molecules, decreasing the photocatalytic

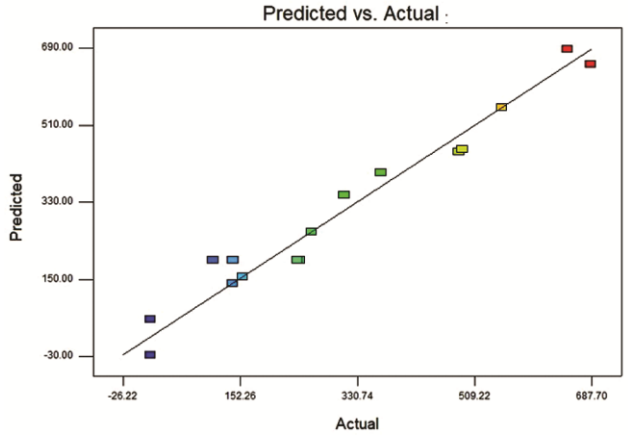

Fig. 8 — Predicted versusactual values for photocatalytic hydrogen production based on as-prepared microspheres from black sand.

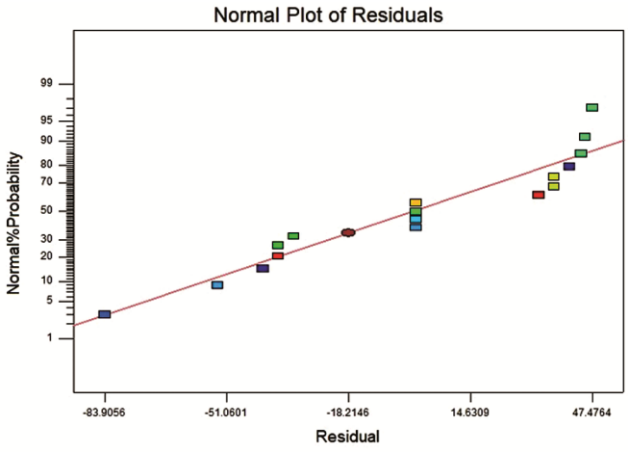

Fig. 9 — Normal probability plots of the residuals for photocatalytic hydrogen production based on as-prepared microspheres from black sand.

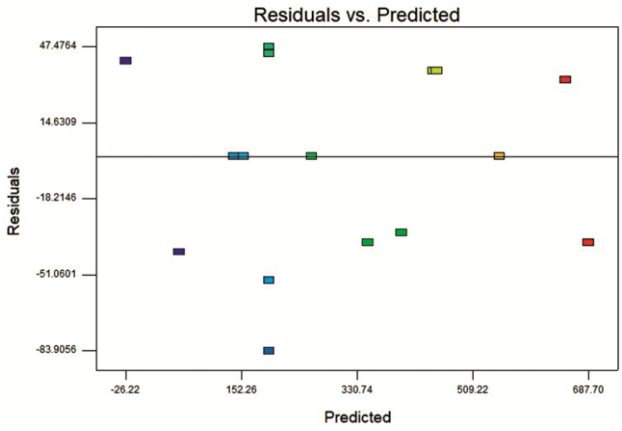

Fig. 10 — Plot of the residuals against the predicted response for photocatalytic hydrogen production based on as-prepared microspheres from black sand.

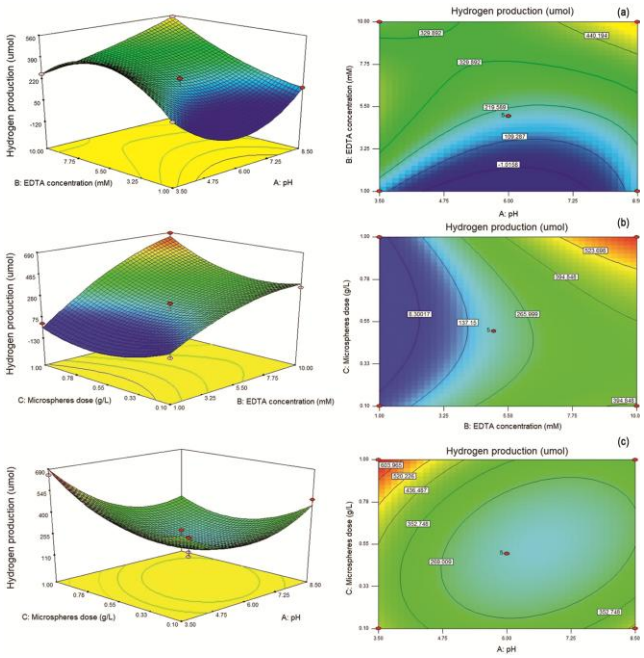

Fig. 11 — Effects of pH, sacrificial agent concentration and microspheres dose on photocatalytic hydrogen production(a) Microspheres dose 0.5 gL^{-1}, (b) pH 6.0 and (c) Sacrificial agent concentration 5.0 mM.

hydrogen production. For this case, the EDTA is partially ionized (negatively charged), while the surface of the microspheres is positively charged promoting the attraction between these species.

3.3 Process Optimization and Model Validation

With the purpose of maximize the hydrogen production using microspheres based on black mineral sand as a semiconductor, the reaction conditions were adjusted according to optimization results determined by statistical analysis. Subsequently, the initial pH was set to 7.2, the EDTA concentration was set to 6.0 mM and the microspheres dose at 1.0 gL^{-1}. The theoretical maximum hydrogen production was 393.44 µmol. Consequently, the experiment conducted with the optimized parameters produced 401.51 µmol. The acceptable fit between predicted and experimental results (relative error ~2.0%), indicated that Box-Behnken design was right to optimize the photocatalytic hydrogen production using microspheres based on black mineral sand as a photocatalyst.

4 Conclusions

For the photocatalyst preparation, a magnetic concentrate obtained from natural ore (black sand composed primarily of iron oxides with a small participation of elements such as Ti, Si, and Al principally) was used, which had a high thermal stability. As-prepared microspheres (MS) were prepared by a simple microencapsulation method using Na-alginate as a polymer matrix. After the calcination process (1100°C), the microspheres had a regular size of 336.61 µm ±35.8, and its sintered structure formed empty spaces associated to porosity (16%). As a consequence of the calcination process, the weight gain observed (<1.0%) until 250°C, could be attributed to some crystallization of magnetite (Fe_3O_4) to γ and α-hematite, while the transformation from γ to the α-hematite phase could have occurred above this temperature. In the XRD pattern of starting magnetic concentrate emerged magnetite, ilmenite, hematite, and quartz phase, while the structure of the as-prepared microspheres revealed the formation of titanium oxide (Ti_3O_5) product of the phase transitions of the mineral. The diffraction peaks of other impurities, such as Na and C from alginate on the microspheres were not observed. The results showed that the magnetite in M1 was oxidized and the main component in MS was hematite (Fe_2O_3). As-prepared microspheres showed a strong absorption peak at 425 nm (visible range) and had direct optical transition corresponding to a band gap of 2.92 eV which, compared with the magnetic concentrate (3.05 eV), decreased slightly with the calcination process. The calcined microspheres exhibited activity for photocatalytic hydrogen production by EDTA solutions under UV light probably due to the combination of the crystalline phases of the main compound (iron oxide) and the slight contribution of minor elements. Based on statistical analysis, a satisfactory empirical model equation was developed using RSM (Box-Benhken design), whereby it was possible to establish the optimization of parameters using the response surface and contour plots. The production of photocatalytic hydrogen using microspheres based on black sand mineral by EDTA solutions under UV light can be enhanced mainly by low levels of initial pH, and high levels of sacrificial agent and microspheres dose. Although the photocatalysis involves a complex interaction of parameters, the analytical results were endured with the phenomenological explanation of the mechanism through the scattering of UV light in the suspension, the activation of active sites, and the electrostatic repulsion between the charge surface of the microspheres and the dissociated EDTA molecules. The simple microencapsulation method of photocatalytic materials and the easy recovery of microspheres from the reaction system might have a wide potential to be exploited in this kind of processes.

References

1 Fujishima A & Honda K, *Nature*, 238 (1972) 37.
2 Yang H, Guo L, Yan W & Liu H,*J Power Sources*, 159 (2006)1305.
3 Esswein A J & Nocera D G,*Chem Rev*, 107(2007) 4022.
4 Anpo M & Takeuchi M,*J Catal*, 216(2003) 505.
5 Martyanov I N, Uma S, Rodrigues S & Klabunde K J, *Chem Commun*, 21 (2004) 2476.
6 Ni M, Leung MK H, Leung D Y C &SumathyK, *Renew Sustain Energy Rev*,11 (2007) 401.
7 Patsoura A, Kondarides D I & Verykios X E, *Cata Today*, 124 (2007) 94.
8 Jiang F, Zheng S, An L & Chen H, *Appl Surf Sci*, 258 (2012)7188.
9 Fuyuki T & Matsunami H, *Jpn J Appl Phys*, 25(1986) 1288.
10 Deng Q R, Xia X H, Guo M L, Gao Y & Shao G, *Mater Lett*, 65 (2011)2051.
11 Tayade R J, Surolia P K, KulkarniR G & Jasra R V, *Sci Technol Adv Mater*, 8(2007) 455.
12 Hanaor D A H & Sorrell C C, *J Mater Sci*, 46 (2011) 855.
13 Simpraditpan A, Wirunmongkol T, Pavasupree S & Pecharapa W, *Mater Res Bull*, 48(2013) 3211.
14 Schoonen M A A, XuY & Strongin D R, *J Geochemical Explor*, 62 (1998) 201.
15 Fujii T, Kayano M, Takada Y, Nakanishi M & Takada J, *Solid State Ionics*, 172(2004) 289.

16 Zhou F, Kotru S & Pandey R K,*Mater Lett*, 57 (2003) 2104.
17 Chen G, Chen J, Guo S, Li J, Srinivasakannan C & Peng J,*Appl Surf Sci*, 258(2012) 4826.
18 Wilson N C, Muscat J, Mkhonto D, NgoepeP E & Harrison N M,*Phys Rev B*, 71 (2005)75202.
19 LaxmiT, Srikant S S, Rao D S & Bhima R R B, *Int J Min Sci Technol*, 23(2013) 725.
20 Klepka M T, Lawniczak-Jablonska K, Wolska A & Jablonski M, *J Electron Spectros Relat Phenomena*, 182(2010) 85.
21 Mehdilo A, Irannajad M & Rezai B, *Colloids Surf A Physicochem Eng Asp*, 428(2013) 111.
22 Beydoun D, Amal R, Low G & McEvoy S, *J Nanoparticle Res*, 1 (1999) 439.
23 Chong M N, Jin B, Chow C W K & Saint C,*Water Res*, 44 (2010)2997.
24 Nakashima T & Kimizuka N,*J Am Chem Soc*, 125 (2003) 6386.
25 Keshmiri M & Troczynski T, *J Non Cryst Solids*, 311(2002) 89.
26 Shiba K, Tagaya M, Tilley R D & Hanagata N, *Sci Technol Adv Mater*, 14 (2013)23002.
27 Yu J, Qi L, Cheng B & Zhao X,*J Hazard Mater*, 160(2008) 621.
28 Song X, Zhao Y, Wang H & Du Q, *Langmuir*, 25 (2009)4443.
29 Lu W, Gao S & Wang J, *J Phys Chem C*, 112 (2008) 16792.
30 Dwivedi C, Raje N, Nuwad J, Kumar M & Bajaj P N, *Chem Eng J*, 193–194(2012) 178.
31 Li H, Liu G, Chen S & Liu Q,*Phys E Low-dimensional Syst Nanostructures*, 42(2010) 1844.
32 Li X, Wu X, He G, Sun J, Xiao W & Tan Y, *Chem Eng J*, 251(2014) 58.
33 Subha N, Mahalakshmi M, Myilsamy M, Lakshmana Reddy N, Shankar MV, Neppolian B & Murugesan V, *Colloids Surf A Physicochem Eng Asp*, 522 (2017)193.
34 Lu L, Ni S, Liu G & Xu X,*Int J Hydrogen Energy*, 42 (2017)23539.
35 Xie TH, Sun X & Lin J,*J Phys Chem C*, 112 (2008) 9753.
36 Lopez-Vasquez A, Delgado-Nino P & Salas-Siado D, *Environ Sci Pollut Res Int*, 26 (2019)4202.
37 Su E C, Huang B S, Liu C C & Wey M Y, *Renew Energy*, 75 (2015) 266.
38 Hinkelmann K & Kempthorne O, Design and Analysis of Experiments, Volume 1: Introduction to Experimental Design (John Wiley & Sons, Inc, New Jersey), 2nd Edn, ISBN: 9780471727569,2007, p. 510.
39 Montgomery D C, Design and Analysis of Experiments(John Wiley & Sons, Inc, New Jersey), 8th Edn. ISBN: 9781118214718, 2012, p. 503.
40 Box GEP, Hunter JS & Hunter W G, Statistics for Experimenters: Design, Innovation, and Discovery(Wiley-Interscience, New Jersey), 2ndEdn. ISBN: 9780471718130, 2005, p. 477.
41 Khuri A I,Response Surface Methodology and Related Topics (World Scientific, New Jersey), 1st Edn. ISBN: 9812564586, 2006, p. 23.
42 Whitcomb P J & Anderson M J, RSM Simplified: Optimizing Processes Using Response Surface Methods for Design of Experiments (Taylor & Francis, New York), 1st Edn. ISBN: 9781563272974, 2004, p. 193.
43 Jo J, *Construction and Properties of Box-Behnken Designs*, Doctoral dissertation, Virginia Tech Virginia Polytechnic Institute and State University, 1992.
44 Myers R H, Montgomery D C & Anderson-Cook C M, Response Surface Methodology: Process and Product Optimization Using Designed Experiments (John Wiley & Sons, Inc, New Jersey), 4thEdn. ISBN: 9781118916018, 2016, p. 415
45 Brereton R G, Chemometrics: Data Analysis for the Laboratory and Chemical Plant(Wiley, West Sussex, England), 1stEdn. ISBN: 0471489778, 2003, p. 76-84
46 Yang Y J & Draper N R,*J Qual Technol*, 35 (2003)294.
47 Keane M P,*J Bus Econ Stat*, 10 (1992)193.
48 López-Vásquez A, Colina J A & Machuca-Martínez F, *Data Br*, 30 (2020) 105373.
49 Mateus A Y P, Barrias C C, Ribeiro C, Ferraz M P & Monteiro F J, *J Biomed Mater Res A*, 86 (2008) 483.
50 López-Vásquez A, Suárez-Escobar A & Ramírez J H, *Chemistry Select*, 5 (2020)252.
51 Wang J, Ma T, Zhang Z, Zhang X, Jiang Y, Sun W, Li R & Zhang P,*Ultrason Sonochem*, 14 (2007) 575.
52 Ding B, Kim H, Kim C, Khil M & Park S,*Nanotechnology*, 14 (2003)532.
53 Xu X, Ji F, Fan Z & He L,*Int J Environ Res Public Health*, 8 (2011) 1258.
54 Jiwei Z, Tao Y, Liangying Z& Xi Y,*Ceram Int*, 25 (1999) 667.
55 Samanta S, Mukherjee S & Dey R, *Trans Nonferrous Met Soc China*, 24 (2014)2976.
56 Ali A, Zafar H, Zia M, Ul H I, Phull AR, Ali JS& Hussain A, *Nanotechnol Sci Appl*, 9 (2016) 49.
57 Kubelka P, *J OptSoc Am*, 38 (1948)448.
58 Mäkelä M, *Energy Convers Manag*, 151 (2017) 630.
59 Dehghannasiri R, Xue D, Balachandran P V, Yousefi M R, Dalton L A & Edwar T L,*Comput Mater Sci*, 129 (2017) 311.